ELSEVIER

Chemical Engineering Journal 136 (2008) 133–143

Chemical Engineering Journal

www.elsevier.com/locate/cej

Thermal fluid dynamics analysis of gas–liquid flow on a distillation sieve tray

D. Noriler [a,*], H.F. Meier [b], A.A.C. Barros [b], M.R. Wolf Maciel [a]

[a] *Laboratory of Separation Processes Development, Chemical Engineering School, State University of Campinas, 13083-970 Campinas, Brazil*

[b] *Laboratory of Computational Fluid Dynamics, Department of Chemical Engineering, Regional University of Blumenau, 89030-000 Blumenau, Brazil*

Received 12 April 2006; received in revised form 9 March 2007; accepted 13 March 2007

Abstract

Conventional models for distillation columns are based on equilibrium and non-equilibrium stage concepts, and both consider the fluid dynamics in a macroscopic point of view. The main objective of this work is to apply a CFD model under Eulerian-Eulerian framework for gas–liquid flows, with capability to predict the momentum and thermal phenomena of the multiphase flows. A three-dimensional and transient model with energy and momentum conservation balances has been applied for predictions of volume fractions, velocities, pressure and temperature fields of two-phase flows on sieve tray distillation. The mathematical model was applied in the CFD commercial code for numerical studies, with the construction of a particular numerical grid and with own sub-routines in FORTRAN language for the closures equations obtained from literature. The model is solved using the finite-volume method with variables located in a generalized co-ordinate system for typical operating conditions taken from the literature. The results show the volume fractions, velocities and temperature profiles as a function of the time and the position in the distillation sieve tray and when are compared with the literature comments confirm that the model is suitable to predict thermal gas–liquid flows on a distillation sieve tray.

Keywords: Distillation; CFD; Modeling; Distillation tray; Gas–liquid flow

1. Introduction

A better understanding, from the microscopic point of view, of the mechanisms that occur in large scale industrial processes is important in order to improve equipment, design and process development. In this way, distillation columns are one of the most important separation techniques. Models to represent the behavior of distillation columns are available in the open literature [1–8]. However, despite the relevant results obtained with equilibrium and non-equilibrium stage models, they neglect the fluid dynamics phenomena assuming perfect mixture on the plates. However, it has been recognized that the flow pattern on a distillation tray is of large importance on the mass transfer efficiency [9,10], and this influence can only be analyzed making a fluid dynamic study.

Recent advances and interest in the use of CFD techniques have allowed the study of fluid dynamic in processes and equipments [11–19]. Contributions have been made in CFD in microscopic modeling and simulation of bubbling gas–solid flow [12–14] of fluidized beds [15,16], among others, besides gas–liquid flows, as for example ozonation towers [17]. Bubble columns have been firstly considered for modeling bubbling flows [19–30], where bubble gas crosses the liquid column, introducing, at the same time, advances for modeling gas–liquid flow on a distillation tray.

Some works on gas–liquid flow on a distillation tray using CFD techniques can be mentioned [31–38]. Mehta et al. [31] have analyzed the liquid phase flow patterns by solving the time-averaging equations of continuity of mass and momentum only for the liquid phase. Liu et al. [32] attempt to model the two-phase flow considering that the liquid phase is the most important, and modeled the gas action with empirical equation. Krishna et al. [33] and van Baten and Krishna [34] suggested a three-dimensional and multiphase model to represent the

* Corresponding author. Tel.: +55 2147 3221 6060; fax: +55 2147 3221.6001.
E-mail address: dnoriler@yahoo.com.br (D. Noriler).

1385-8947/$ – see front matter © 2007 Elsevier B.V. All rights reserved.
doi:10.1016/j.cej.2007.03.023

Nomenclature

A	interfacial area per volume (m^2/m^3)
A_B	active bubbling area (m^2)
A_H	holes area (m^2)
C_D	drag coefficient
C_p	specific heat of fluid (J/kg K)
C_μ, C_1, C_2	turbulence model constants
d	hole diameter (m)
d_g	bobble diameter (m)
D	column diameter (m)
f	volume fraction
$\mathbf{g}$	gravity vector (m/s^2)
h	enthalpy (J/kg)
h_{gl}	global heat transfer coefficient (J/s m^2 K)
h_w	weir height (m)
i	turbulence intensity
k	turbulent kinetic energy (m^2/s^2)
Ls	dissipation length scale (m)
M_{gl}	interphase momentum exchange term (N/m^3)
P	pressure (N/m^2)
$\mathbf{P}$	shear production (N/s)
Pr	Prandtl number
Q_l	rate of liquid flow (m^3/s m)
Q_{gl}	interphase energy exchange term (J/s m^3)
Re	Reynolds number
t	time (s)
U_g	superficial gas velocity (m/s)
$\mathbf{v}$	velocity vector (m/s)
W	weir length (m)
x	co-ordinate (m)
y	co-ordinate (m)
z	co-ordinate (m)

Greek letters

ε	dissipation rate of turbulence kinetic energy (m^2/s^3)
λ	thermal conductivity (J/s m K)
μ	viscosity (kg/m s)
ρ	density (kg/m^3)
σ^ε, σ^k	turbulence model constants
ξ	orthogonal direction to the wall

Subscripts

eff	effective property
g	gas phase
in	inlet
k	kth phase
l	liquid phase
out	outlet
x	co-ordinate x
y	co-ordinate y
z	co-ordinate z
t	turbulent property
eff	effective property
0	initial value

hydrodynamics on a distillation sieve tray. The authors use the Eulerian-Eulerian framework and the Reynolds Averaged Navier-Stokes (RANS) equations for modeling turbulent gas–liquid flows assuming that momentum exchange considers only bubble–liquid interaction, i.e., the bubble–bubble interaction was not considered. Soares et al. [35] attempt to model the two-phase flow behavior considering that the drag force between phases is very high for distillation cases. This implicates that the gas and the liquid velocities are the same. The authors showed a comparison between heterogeneous (van Baten & Krishna [34]) and homogeneous models for free surface flow and bubble columns. Noriler and coworkers [35] proposed to use the homogeneous model for predicting the hydrodynamic on a distillation sieve tray. Gesit et al. [37] applied the heterogeneous model for commercial-scale sieve tray and compared the results with experimental data obtained by Solari and Bell [10]. Nevertheless, the energy and mass conservations are neglected in most of the works. Component mass conservation is applied in bubbling flow by some authors [17,20,30], however, the energy conservation is not available.

In this work, we have implemented a CFD model under Eulerian-Eulerian framework for gas–liquid flows, with capability to predict the main phenomenological aspects of multiphase flows. The three-dimensional and transient model, with mass continuity, and energy and momentum conservations, has been applied for predicting the volume fractions, velocities, pressure and temperature fields, of the two-phase flow on the distillation sieve trays. The model is solved using finite-volume method with variables located in a generalized co-ordinate system, for typical operating conditions taken from the literature.

2. Mathematical model

The model considers the flows of gas and liquid in Eulerian-Eulerian framework, where each phase is treated as interpenetrating continuum having separate transport equations. Therefore, the Reynolds Averaged Navier-Stokes equations (RANS) for the gas phase (subscript g) and for the liquid phase (subscript l) can be written as follow.

2.1. Mass continuity equations

Gas phase

$$\frac{\partial}{\partial t}(f_g\rho_g) + \nabla \times (f_g\rho_g\mathbf{v}_g) = 0 \quad (1)$$

Liquid phase

$$\frac{\partial}{\partial t}(f_l\rho_l) + \nabla \times (f_l\rho_l\mathbf{v}_l) = 0 \quad (2)$$

where f_k, ρ_k and $\mathbf{v}_k$ represent the volume fraction, macroscopic density and velocity vector for kth phase, respectively.

The gas and liquid volume fractions, f_g and f_l, are related through the summation constraint:

$$f_g + f_l = 1$$

2.2. Momentum equations

Gas phase

$$\frac{\partial}{\partial t}(f_g\rho_g\mathbf{v}_g) + \nabla\times(f_g\rho_g\mathbf{v}_g\mathbf{v}_g) = -f_g\nabla P_g + \nabla\times[f_g\mu_g(\nabla\mathbf{v}_g + \nabla\mathbf{v}_g^T)] + M_{gl} + \rho_g f_g\mathbf{g} \quad (3)$$

Liquid phase

$$\frac{\partial}{\partial t}(f_l\rho_l\mathbf{v}_l) + \nabla\times(f_l\rho_l\mathbf{v}_l\mathbf{v}_l) = -f_l\nabla P_l + \nabla\times[f_l\mu_l^{Eff}(\nabla\mathbf{v}_l + \nabla\mathbf{v}_l^T)] - M_{gl} + \rho_l f_l\mathbf{g} \quad (4)$$

where μ_k and $\mathbf{g}$ represent the molecular viscosity for kth phase and the gravity vector, respectively. P_k is the pressure field, having the same value for the gas and for the liquid phase, i.e., $P_g = P_l$. The M_{gl} represents the momentum transfer between the gas and the liquid phases and the additional flux of momentum due to the velocity fluctuation, turbulence, was incorporated in the diffusion term.

2.3. Energy equation

Gas phase

$$\frac{\partial}{\partial t}(f_g\rho_g h_g) + \nabla\times(f_g\rho_g\mathbf{v}_g h_g) - \nabla\times(f_g\lambda_g\nabla T_g) = +Q_{gl} \quad (5)$$

Liquid phase

$$\frac{\partial}{\partial t}(f_l\rho_l h_l) + \nabla\times(f_l\rho_l\mathbf{v}_l h_l) - \nabla\times(f_l\lambda_l^{Eff}\nabla T_l) = -Q_{gl} \quad (6)$$

where h_k and T_k represents the enthalpy and temperature for kth phase, respectively. Q_{gl} represents the energy transfer between the gas and the liquid phases and additional flux of energy due to the velocity and the enthalpy fluctuation was incorporated in the diffusion term.

2.4. Closure equations

For solving Eqs. (1)–(6), it is necessary additional equations relating the interphase momentum transfer, M_{gl}, interphase energy transfer, Q_{gl}, and additional fluxes for momentum and energy.

2.4.1. Interphase momentum transfer

For the interphase momentum transfer, we consider that the momentum transfer is only due to the drag force. The drag force per unit volume can be written as:

$$M_{gl} = \frac{3}{4}\frac{f_g\rho_l}{d_g}C_D|\mathbf{v}_g - \mathbf{v}_l|(\mathbf{v}_g - \mathbf{v}_l) \quad (7)$$

where d_g is the bubble diameter and C_D is the drag coefficient.

The drag coefficient, C_D, has been estimated using the drag correlation of Krishna et al. [33], proposed for the rise of a swarm of large bubbles in the churn turbulent regime:

$$C_D = \frac{4}{3}\frac{\rho_l - \rho_g}{\rho_l}gd_g\frac{1}{|\mathbf{v}_g - \mathbf{v}_l|^2} \quad (8)$$

In this equation, $|\mathbf{v}_g - \mathbf{v}_l|$ is the relative velocity between the gas and the liquid phases and it can be estimated as a function of the gas superficial velocity, $U_g = Q_G/A_B$, and of the gas average holdup, $f_g^{average}$, as following:

$$|\mathbf{v}_g - \mathbf{v}_l| = \frac{U_g}{f_g^{average}} \quad (9)$$

For the gas average holdup, we used the Bennett et al. [7] correlation:

$$f_\beta^{average} = 1 - \exp\left[-12.55\left(U_g\sqrt{\frac{\rho_g}{\rho_l - \rho_g}}\right)^{0.91}\right] \quad (10.1)$$

Making proper substitution and simplifying the interphase momentum transfer, it can be rewritten in a form suitable for CFD use (van Baten and Krishna [34]):

$$M_{gl} = f_g(\rho_l - \rho_g)g\left[\frac{1}{(U_g/f_g^{average})^2}\frac{1}{(1 - f_g^{average})}\right] \times(\mathbf{v}_g - \mathbf{v}_l)|\mathbf{v}_g - \mathbf{v}_l| \quad (11)$$

Note that in Eq. (11), the bubble diameter is not present, eliminating, thus, the main problem for prediction of gas liquid bubbling flow.

2.4.2. Interphase energy transfer

The energy rate that crosses the interface between gas and liquid phases can be described as:

$$Q_{gl} = h_{gl}A_g(T_g - T_l) \quad (12)$$

where h_{gl} is the global heat transfer coefficient, A_g is the interfacial area per volume unit and it can be calculated by $A_g = 6f_g/d_g$.

The global heat transfer coefficient is defined as (Bird et al. [38]):

$$h_{gl} = \frac{\lambda_g Nu_{gl}}{d_g} \quad (13)$$

where λ_g is the thermal conductivity and Nu_{gl} is the Nusselt number. Nusselt number for spherical bubble in turbulent regime can be calculated by Ranz and Marshall [39] equation:

$$Nu_{gl} = 2.0 + 0.6Re_g^{0.5}Pr_g^{0.3} \quad \text{for} \quad 0 \le Re_g \le 200 \quad \text{and} \quad 0 \le Pr_g \le 250 \quad (14)$$

with particle Reynolds and Prandtl numbers, Re_g and Pr_g, defined as:

$$Re_g = \frac{\rho_l\mathbf{v}_g d_g}{\mu_l}; \quad Pr_g = \frac{\mu_g C_{p_g}}{\lambda_g}$$

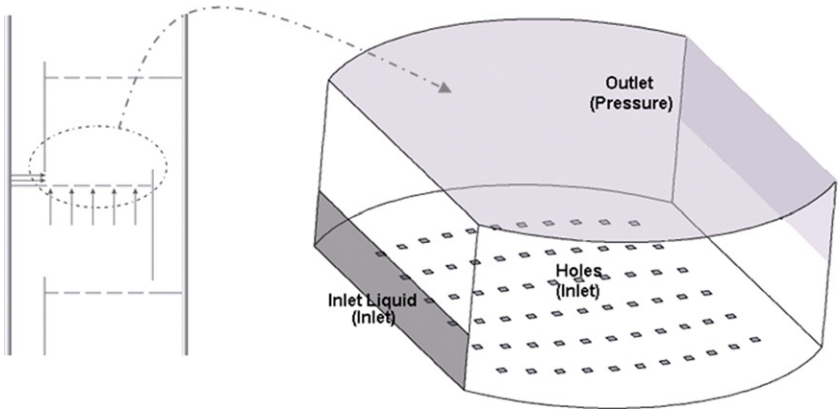

Fig. 1. Flow geometry and boundary conditions.

2.4.3. Turbulence equations

By application of the time average procedure in the Navier Stokes equations, an extra term appears due to the turbulent fluctuation of the velocities, which needs to be represented by a constitutive equation. This term is known as Reynolds stress, for the additional momentum flux, and Reynolds flux, for more equations. If we consider that the fluctuations (turbulence) consists of small swarms to be formed and to be dispersed, and that the Reynolds stresses can be linearly related to the mean velocity gradients (eddy viscosity hypothesis) similar to the relationship between the stress and the strain tensors in laminar Newtonian flow, an effective viscosity can be assumed:

$$\mu^{\mathrm{Eff}} = \mu + \mu_{\mathrm{t}}$$

and the Reynolds fluxes of a scalar are linearly related to the mean scalar gradient (eddy diffusivity hypothesis). This implies in:

$$\lambda^{\mathrm{Eff}} = \lambda + \frac{\mu_{\mathrm{t}}}{Pr_{\mathrm{t}}} \equiv \text{for the additional term in energy equation}$$

It can be used the standard k-ε turbulence model for representing the additional flux term. Pr_{t} is the turbulent Prandtl number and μ_{t} is the turbulent viscosity.

The standard k-ε model is connected with the turbulent kinetic energy and its dissipation rate as following:

$$\mu_{\mathrm{t}} = C_{\mu}\rho\frac{k^2}{\varepsilon} \tag{15}$$

where k is the turbulent kinetic energy and ε is the dissipation rate of turbulent kinetic energy. The conservation equation for turbulent kinetic energy and its dissipation rate can be written as:

$$\begin{aligned}
&\frac{\partial}{\partial t}(f_{\mathrm{l}}\rho_{\mathrm{l}}k_{\mathrm{l}}) + \nabla\times\left\{f_{\mathrm{l}}\left[\rho_{\mathrm{l}}\mathbf{v}_{\mathrm{l}}k_{\mathrm{l}} - \left(\mu_{\mathrm{l}} + \frac{\mu_{\mathrm{t}}}{\sigma_{\mathrm{k}}}\right)\nabla k_{\mathrm{l}}\right]\right\} = f_{\mathrm{l}}(\mathbf{P} - \rho_{\mathrm{l}}\varepsilon_{\mathrm{l}})\\
&\frac{\partial}{\partial t}(f_{\mathrm{l}}\rho_{\mathrm{l}}\varepsilon_{\mathrm{l}}) + \nabla\times\left\{f_{\mathrm{l}}\left[\rho_{\mathrm{l}}\mathbf{v}_{\mathrm{l}}\varepsilon_{\mathrm{l}} - \left(\mu_{\mathrm{l}} + \frac{\mu_{\mathrm{tl}}}{\sigma_{\varepsilon}}\right)\nabla\varepsilon_{\mathrm{l}}\right]\right\} = f_{\mathrm{l}}\frac{\varepsilon_{\mathrm{l}}}{k_{\mathrm{l}}}(C_1\mathbf{P} - C_2\rho_{\mathrm{l}}\varepsilon_{\mathrm{l}})
\end{aligned} \tag{16}$$

with

$$\mathbf{P} = \mu_{\mathrm{t}}\nabla\mathbf{v}_{\mathrm{l}}\times[\nabla\mathbf{v}_{\mathrm{l}} + (\nabla\mathbf{v}_{\mathrm{l}})^{\mathrm{T}}]$$

where C_{μ}, C_1, C_2, σ_{k} and σ_{ε} are the model constants.

The gas phase is considered in laminar regime. It can be shown that the turbulent kinetic energy associated with the gas phase represents 0.1% of the turbulent kinetic energy; therefore, there are no conservation equations for k and ε in this phase.

2.5. Boundary and initial conditions

Due to the elliptical characteristics of the partial differential equations of the model, boundary conditions of all frontiers of the physical domain are necessary: at the inlet, uniform profile of velocities and turbulent properties are imposed; no slip conditions on the wall for both phases; and pressure conditions in the outlet were also applied for the two phases. Fig. 1 shows the physical domain used in the simulations.

The conditions can be written in a mathematical form according to Table 1.

Air, at ambient pressure, and water were used as the gas and liquid phases, respectively. At the beginning of the simulation, the conditions consist of to fill up liquid until the weir height, and air up to the weir height at homogeneous temperature equal to T_0. The velocity fields and the turbulent properties were also considered as initial conditions to close up the model. Details about the initial conditions for each simulation will be shown below.

3. Numerical methods and geometry flow

Finite volume method was used to solve the partial differential equations, with a structured multi-block grid generated by the body fitted on generalized and collocated grid. The HYBRID interpolation scheme was used with pressure–velocity coupling obtained using SIMPLEC algorithm. The improved RHIE-CHOW algorithm was used to calculate the velocity at the cell faces to avoid numerical problems like check-boarding and zigzag. The relation factors were not used. The commercial code CFX 4.4 by ANSYS was used to generate the grids, to

Table 1
Boundary conditions

Boundary conditions	Properties	Liquid phase	Gas phase
Inlet liquid (inlet)	$v_x\|_{in} = \dfrac{Q_l}{h_w}, \quad v_y\|_{in} = 0, \quad v_z\|_{in} = 0$	$f_{l,in} = f_{l0}$	$f_{g,in} = 1 - f_{l,in}$
	$k\|_{in} = 1.5(i \times v_x)^2, \quad \varepsilon\|_{in} = \dfrac{(k\|_{x=0})^{1.5}}{0.3\,Ls}$	$T_{l,in} = T_{l0}$	$T_{g,in} = T_{g0}$
Holes (inlet)	$v_x\|_{in} = 0, \quad v_y\|_{in} = 0, \quad v_z\|_{in} = V_S \dfrac{A_B}{A_H}$	$f_{l,in} = f_{l0}$	$f_{g,in} = 1 - f_{l,in}$
	$k\|_{in} = 1.5(i \times v_x)^2$	$T_{l,in} = T_{l0}$	$T_{g,in} = T_{g0}$
	If inflow $\left.\dfrac{\partial \mathbf{v}_l}{\partial \zeta}\right\|_{out} = \left.\dfrac{\partial \mathbf{v}_g}{\partial \zeta}\right\|_{out} = 0, \quad k = k_{out}; \varepsilon = \varepsilon_{out} \quad P_{static}\|_{out} = P_0$	$f_{l,out} = 0$	$f_{g,out} = 1$
Outlet (pressure)		$T_l = T_{l,out}$	$T_g = T_{g,out}$
	If Outflow $\left.\dfrac{\partial v_l}{\partial \zeta}\right\|_{out} = \left.\dfrac{\partial v_g}{\partial \zeta}\right\|_{out} = 0, \quad \left.\dfrac{\partial k}{\partial \zeta}\right\|_{out} = \left.\dfrac{\partial \varepsilon}{\partial \zeta}\right\|_{out} = 0 \quad P_{static}\|_{out} = P_0$	$\left.\dfrac{\partial f_l}{\partial \zeta}\right\|_{out} = 0$	$\left.\dfrac{\partial f_g}{\partial \zeta}\right\|_{out} = 0$
		$\left.\dfrac{\partial T_l}{\partial \zeta}\right\|_{out} = 0$	$\left.\dfrac{\partial T_g}{\partial \zeta}\right\|_{out} = 0$
Wall (wall)	$v\|_{wall} = 0, \quad k\|_{wall} = \left.\dfrac{\partial k}{\partial \zeta}\right\|_{wall} = 0$	$\left.\dfrac{\partial f_l}{\partial \zeta}\right\|_{wall} = 0$	$\left.\dfrac{\partial f_g}{\partial \zeta}\right\|_{wall} = 0$
	The wall function was used near wall regions.	$q_l = 0$	$q_g = 0$

ζ is the orthogonal direction to the boundary; the wall functions were standard function of the CFX code.

solve the models and to analyze the results. All calculations of this work were performed on a PC Pentium IV 3.0 GHz. A typical simulation took about 10 days to simulate nearly 20.00 s of tray hydrodynamics, with time increment of 0.002 s.

The geometry and the grid were generated with the pre-processor BUILD from CFX 4.4 by ANSYS. The maximum edge for the finite volumes was fixed in 5 mm to certify the independence of the solution with the grid size. Fig. 2 shows a typical grid used in this work.

4. Results and discussions

4.1. Momentum transfer analyses

The first analysis consists on verifying the momentum transfer model applied, comparing the clear liquid height prediction with those from Bennett et al. [7] and Colwell [6] correlations. A distillation sieve tray with 0.35 m diameter, D, and 0.234 m weir length, W, was used. The column has a rectangular entrance for the liquid with 0.234 m × 0.040 m. The weir height, h_w, is 0.06 m, and the fractional holes area to bubbling area, A_H/A_B, is 0.0227. The length between the entrance and the outlet is 0.260, with 66 holes in the tray.

All simulations were carried out for analyzing the model accuracy, with the superficial gas velocity varying between 0.227 and 0.567 m/s. In the first simulation, the velocity fields and turbulent properties were considered nulls. For other simulations, the final results of each simulation were used as initial conditions to the next case.

During the simulations, the average liquid holdup in the dispersion is monitored and the periodical steady state was obtained after 15.0 s, when the velocity fields and turbulent properties were also considered nulls and after half of time, about real 8.0 s, when the initial conditions used were the final results of the previous simulation. Fig. 3 shows the average liquid holdup versus time with a liquid weir load, Q_l/W, equal to 2.135×10^{-3} m^3/s m

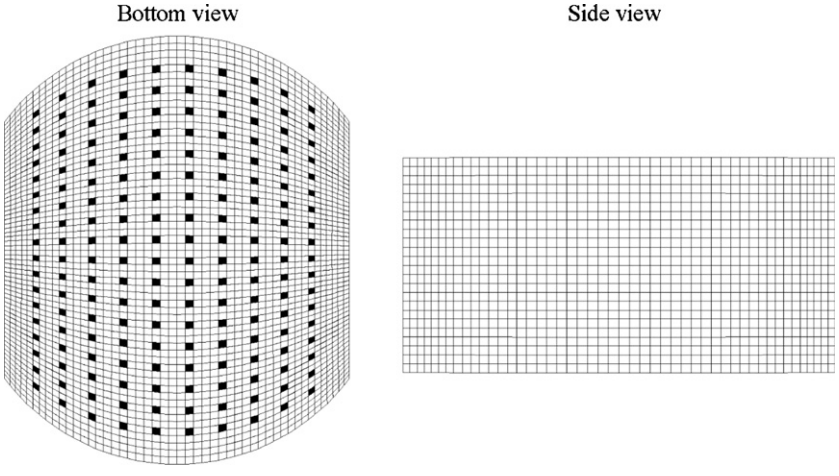

Fig. 2. Typical numerical grid.

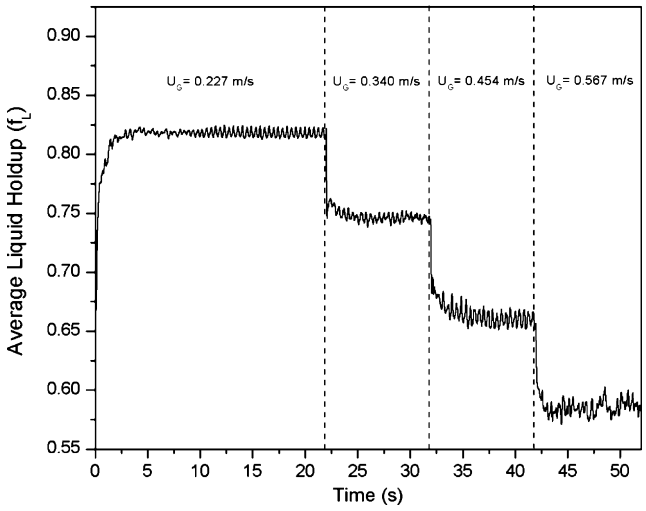

Fig. 3. Transient average liquid holdup for liquid weir load, Q_l/W, equal to 2.135×10^{-3} m^3/s m and the superficial gas velocity between 0.227 and 0.567 m/s.

and the superficial gas velocity between 0.227 and 0.567 m/s. Note that with the increase of the superficial gas velocity, the fluctuation of the average liquid holdup with the time is amplified. This is caused by the increase of the turbulence promoted by the gas in the gas–liquid dispersion.

Fig. 4 shows the comparison of the clear liquid height results between the CFD model and the Bennett et al. [7] and Colwell [6] correlations in function of superficial gas velocity for liquid weir load, Q_l/W, equal to 2.135×10^{-3} m^3/s m. The clear liquid height was calculated by average over a long time to warrant the mean values. The bars in the simulations data represent the standard deviation of the fluctuation of the clear liquid height with the time. It can be noted that the clear liquid height, generated from the volume fraction field, decreases increasing the gas superficial velocity, what agrees with experimental analyses [6,7,10,33]. This phenomenon is due to the increase of bubbling caused by the gas superficial velocity increasing. When

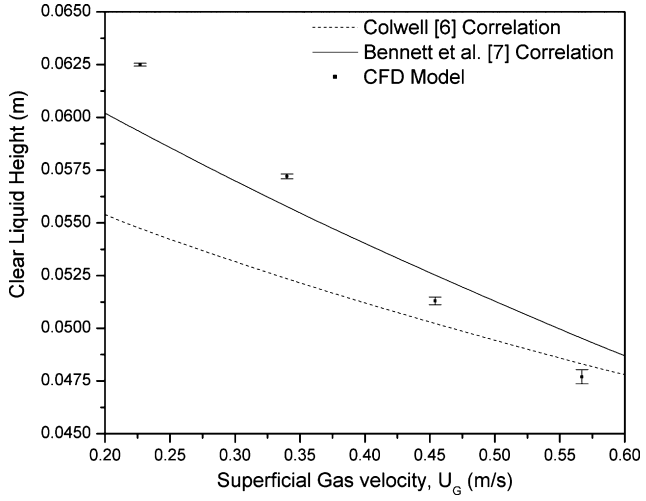

Fig. 4. Clear liquid height for liquid weir load, Q_l/W, equal to 2.135×10^{-3} m^3/s m and the superficial gas velocity between 0.227 and 0.567 m/s.

the CFD model is compared with the correlations used here, it can be seen as better agreement of Bennett correlation due to the fact that since it was developed under the same simulation conditions, i.e., using water and air as continuous and disperse phases, respectively, and under room pressure, presents absolute and relative errors smaller than the Colwell correlation [7]. On the other hand, it can be seen that the simulation data present larger sensitivity to gas superficial velocity. This is expected, since the Bennett correlation is only a function of gas superficial velocity, of weir and of phase physical properties. On the other way, the applied CFD model considers the geometry complexities, the dependence of all flow conservative properties in space and time, besides phase physical properties. So, system physical and geometric characteristics can be associated to phase flow behavior in distillation sieve trays. Furthermore, the applied CFD model holds the theoretical characteristic of the physical phenomena, while the correlation is based on empirism, making restrictive its applicability. Based on this analysis, it is possible to conclude that the model can more robustly represent the characteristic of the liquid gas flow in distillation sieve trays. However, this must be confirmed through experiments. Similar results were obtained by Krishna et al. [33] and van Baten and Krishna [34].

4.2. The inlet boundary condition

In the previous analyses, it was considered a uniform gas velocity in the 66 holes, nevertheless, the gas velocity in each hole may not be the same because the pressure drop in each hole is unequal caused by the fluid dynamics. In order to verify this influence on the flow pattern, it will be considered an extended geometry, where the gas inlet is under the tray. Fig. 5 shows the details of the geometry.

The domain consists of a distillation sieve tray with 0.300 m in diameter, D, and 0.180 m length of the weir, W. The liquid entrance is a rectangular opening with 0.180 m × 0.015 m. The weir height has 0.080 m, h_w, and the fractional holes area to bubbling area, A_H/A_B, is 0.0654. The length from entrance up to outlet is 0.240 m, with 180 holes.

The number of finite elements increases in the extended geometry about 100%, but the maximum edge was maintained in 5 mm, and consequently the computational time increases.

Two simulations were carried out in order to evaluate the influence of the gas boundary condition on the flow patterns: a simulation with simplified geometry and a simulation with extended geometry. Both analyses consider the liquid weir load equal to 1.2×10^{-3} m^3/s m, and the superficial gas velocity equal to 0.7 m/s. The initial conditions of velocity fields and of turbulent properties were considered nulls.

Fig. 6 shows the gas velocity profile in a line above the center holes in the liquid flow direction (Fig. 6a) and above the center holes perpendicular to the liquid flow direction (Fig. 6b), 0.001 m above the tray, for the extended geometry. It is possible to verify changes of the gas velocity in the holes with the position and with the time.

Analyzing Fig. 6a, it can be noted that the gas velocity in the holes in the liquid flow direction changes with the time and the

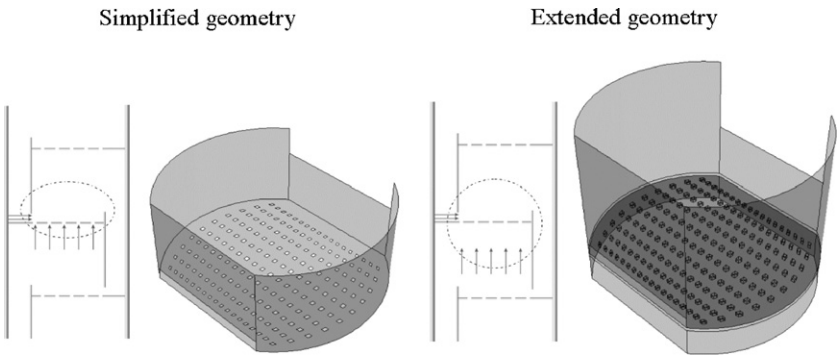

Fig. 5. Geometry and boundary conditions for simplified and extended geometry.

geometrical position (x direction) but it does not present regions with larger gas velocity (there are not maximum, only oscillations). In the regions next to the liquid entrance and to the weir, the gas velocity oscillations in the holes are smaller than those in the other regions, due to the fact that these regions present recirculation zones and high liquid holdup, being more visible than gas oscillations. This was expected, confirming, then, the capacity of the model in representing the phenomenological characteristic of this kind of flow. On the other hand, Fig. 6b shows that the central regions of the tray present larger velocity when compared with the regions near to the wall. These larger velocity peaks are dislocated from the right to the left throughout the time in a region between 30% and 60% of the tray diameter. This oscillation promotes an average parabolic profile, enabling to conclude that, as a function of the larger relative velocity between the phases originated in the central region, a larger drag

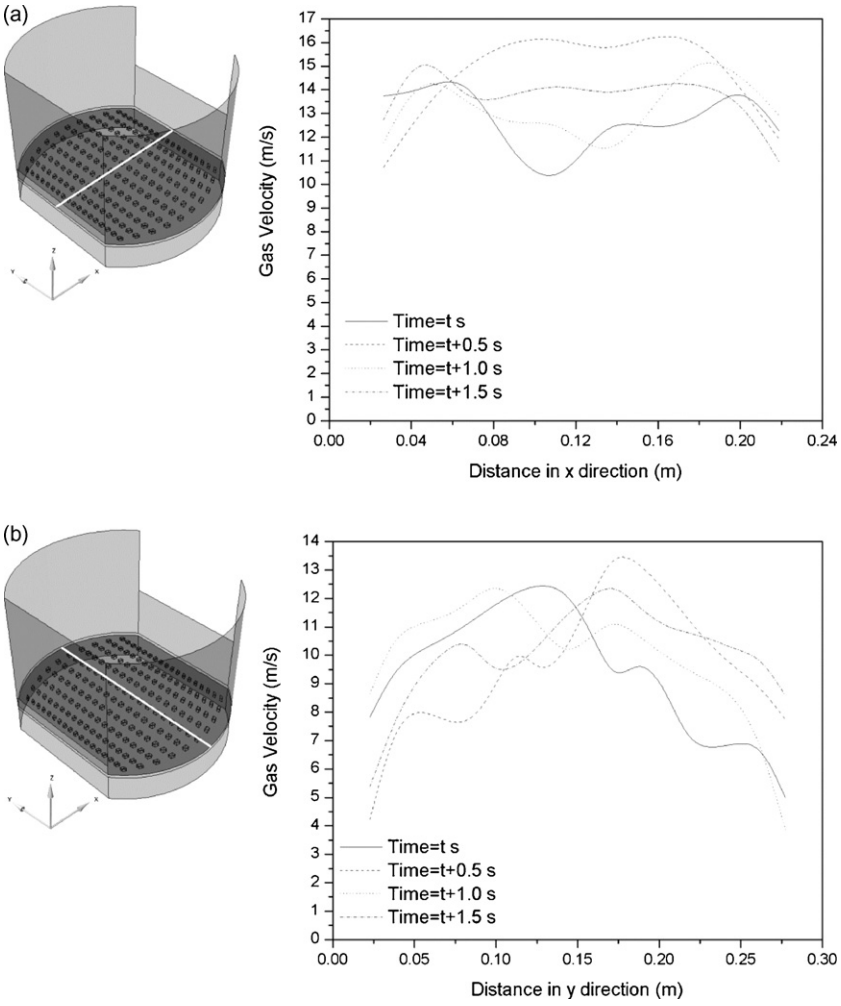

Fig. 6. Gas profile in line above the center holes, 0.001 m above tray for liquid weir load, Q_l/W, equal to 1.2×10^{-3} m^3/s m and the superficial gas velocity, U_g, equal 0.7 m/s: (a) in the direction of the flow; (b) perpendicular to the flow direction.

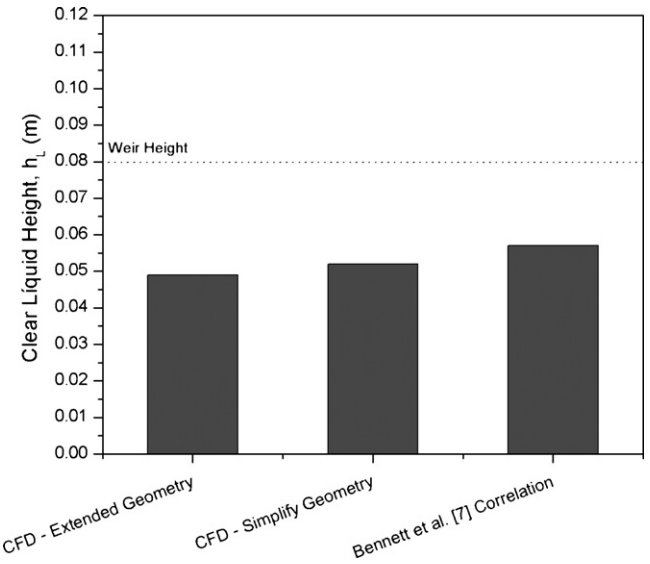

Fig. 7. Comparison of the clear liquid height between simplified and extended geometries and Bennett et al. [7] correlation for liquid weir load, Q_l/W, equal to 1.2×10^{-3} m^3/s m and the superficial gas velocity, U_g, equal to 0.7 m/s.

force is performed and, consequently, smaller liquid holdup and clear liquid height are observed. The main agent of these effects is the gas pressure drop that away from the center is large due to the wall effect, to the absence of holes and to the high liquid holdup.

The effect of the assumption that same gas velocity in all holes on the clear liquid height parameter can be seen in Fig. 7. The results show the comparisons of the clear liquid height among the simplified, and the extended geometries and the Bennett correlation.

It can be seen that the clear liquid height is smaller for the extended geometry than for the simplified one, confirming the previous analyses. The characteristic of dynamic regime of the clear liquid height is maintained for both geometries. The larger gas velocity in the center region of the tray causes this effect because the drag force increases increasing the gas velocity. Consequently, the average liquid volume fraction decreases together with the clear liquid height. Despite the clear liquid height is smaller for the extended geometry than for the simplified one, this divergence is about 4% and it does not promote considerable modifications. This affirmation can be confirmed by the velocity fields.

Fig. 8 shows the vector plot for the simplified and for the extended geometries with liquid weir load, Q_l/W, equal to 1.2×10^{-3} m^3/s m and the superficial gas velocity, U_g, equal to 0.7 m/s in time t. The details in Fig. 8 represent the mainstream lines in both cases.

A similar dynamic behavior can be seen in both cases, with circulating zones next to the entrance and to the weir. However, the flow patterns for the extended geometry shows the liquid raising more intensively in the center than in other regions of the plate, according to Fig. 8. The larger gas velocity in the center regions of the tray induces this tendency.

In Figs. 7 and 8, it is possible to observe small changes in the flow behavior between the studied geometries. However, these changes are not significant and they do not provide further information for the understanding of the evaluated phenomena in distillation sieve tray. It is also important to point out that the computational effort for the extended geometry increases about 100% when compared with the simplified one. So, it is possible to conclude that the hypothesis of the same velocity in all holes is valid and it can be applied for the gas–liquid flow analysis in distillation sieve tray. On the other hand, Fig. 6 shows the hole velocity oscillations as a function of position and time, which, although not expressive, are expected. This implies in a second important conclusion of this analysis, that is, the applied model is able to predict the phenomena associated with gas–liquid flow in a distillation sieve tray, once the predictions agree with an intuitive analysis of these flows.

4.3. Energy analyses—non isothermal flow

The thermal analyses of the gas–liquid flow on a distillation tray are very important to clarify the distillation column dynamic and efficiency, among others. The initial condition for the thermal simulation of the simplified geometry consists of velocity and volume fraction fields and turbulent properties. Other properties were considered in established regime, obtained through the isothermal simulation for liquid weir load, Q_l/W, equal to 1.2×10^{-3} m^3/s m and the superficial gas velocity, U_g, equal to 0.7 m/s, and homogeneous temperature fields, for gas and liquid, equal to 298.15 K. The feed liquid temperature is 298.15 K and for the gas is 318.15 K. The periodical steady state is obtained at around 25.0 s from the started simulation.

Fig. 9 shows the snapshots of liquid temperature in the x–z plane for three different times in the periodical steady state region, for liquid weir load, Q_l/W, equal to1.2×10^{-3} m^3/s m at 298.15 K and the superficial gas velocity, U_g, equal to 0.7 m/s at 318.18 K.

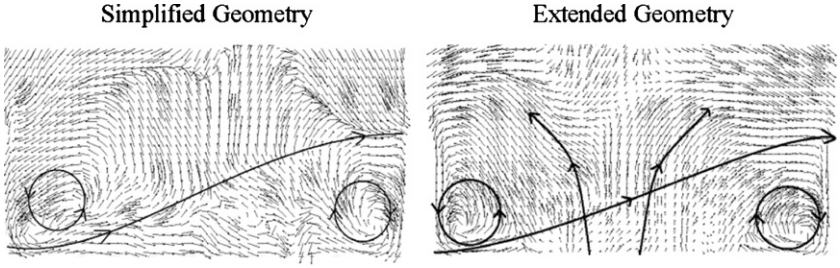

Fig. 8. Liquid velocity fields for liquid weir load, Q_l/W, equal to 1.2×10^{-3} m^3/s m and the superficial gas velocity, U_g, equal to 0.7 m/s.

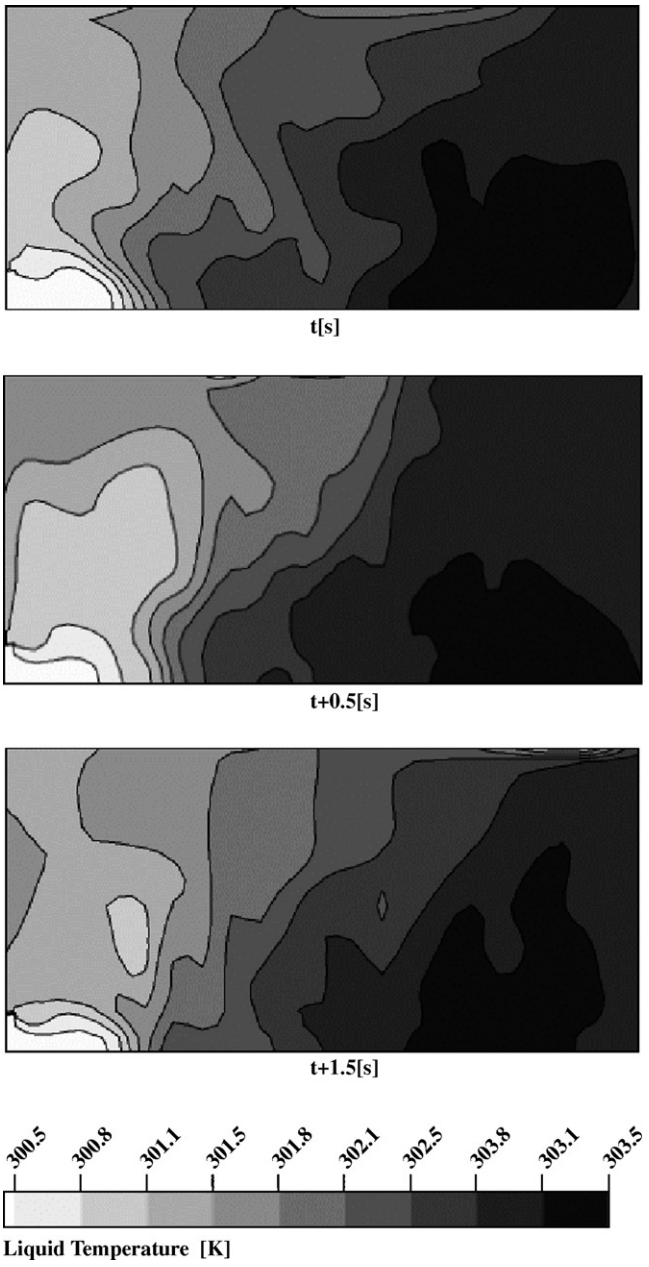

Fig. 9. Snapshots of liquid thermal dynamics in the x–z plane in the periodical steady state region, for liquid weir load, Q_l/W, equal to 1.2×10^{-3} m^3/s m at 298.15 K and the superficial gas velocity, U_g, equal to 0.7 m/s at 318.18 K.

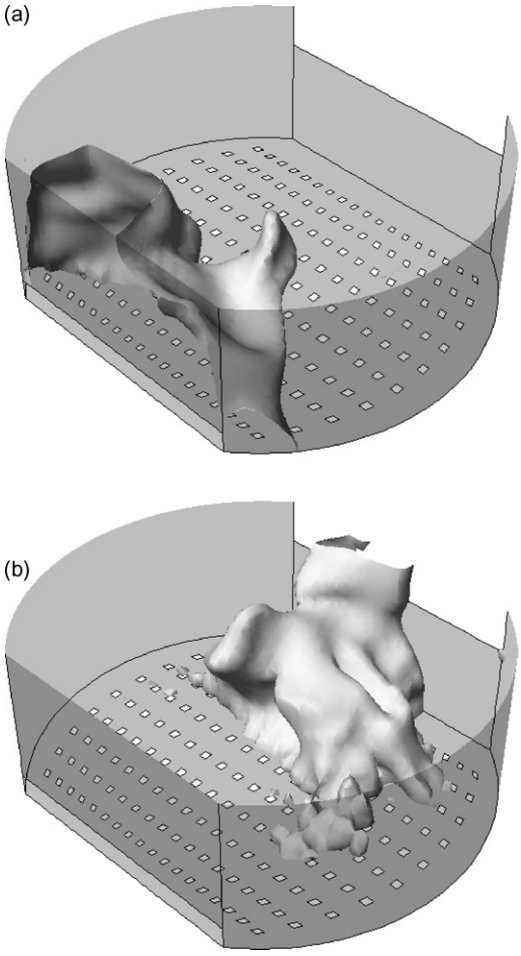

Fig. 10. Isosurfaces of liquid temperature for liquid weir load, Q_l/W, equal to 1.2×10^{-3} m^3/s m at 298.15 K m and the superficial gas velocity, U_g, equal to 0.7 m/s at 318.18 K: (a) temperature equal to 301.45 K; (b) temperature equal to 303.00 K.

It is possible to verify in Fig. 9 that the hot gas enters through the holes, crosses the gas liquid dispersion and changes energy with the liquid. It can be noted a hot region near to the weir due to the cold liquid that enters in the tray. It can be noted that the liquid temperature fields also present a chaotic behavior, similar to the velocity and to the volume fraction profiles, but with a smaller intensity. This effect is due to the high heat transfer rate, caused by the lower resistance to the heat transfer.

Intending to demonstrate more clearly the hot and cold regions of the distillation tray from the three dimensional point of view, Fig. 10 presents isosurfaces for temperature equal to 301.45 K (Fig. 10a) and equal to 303.0 K (Fig. 10b). The cold region near to the liquid inlet and a hot region near to the weir are clearly evident in Fig. 10. The gradient of temperature between the isosurfaces is about 1.45 K, which can be considered representative when observed in terms of temperature influence on the mass transfer since it is directly related to thermodynamic equilibrium.

Fig. 11 shows the average liquid temperature in a y–z plane as a function of x direction. The liquid temperature was determined in the y–z planes at interval of the 0.005 m by averaging over each plane.

As previously, the dependence of the liquid temperature on the position, mainly in the liquid flow direction, should be noted. For the other directions, this dependence was not identified. The small peaks presented in Fig. 11 represent points with higher temperature, because these are the means calculated in planes localized over the holes which have the tendency to present higher temperature.

Through the analysis of the non-isothermal flow, it was possible to establish its importance and the main methodological aspects of the numerical solution for the thermal fluid dynamic model. Thus, it was possible to identify the flow characteristics related to heat transfer, which makes possible to analyse

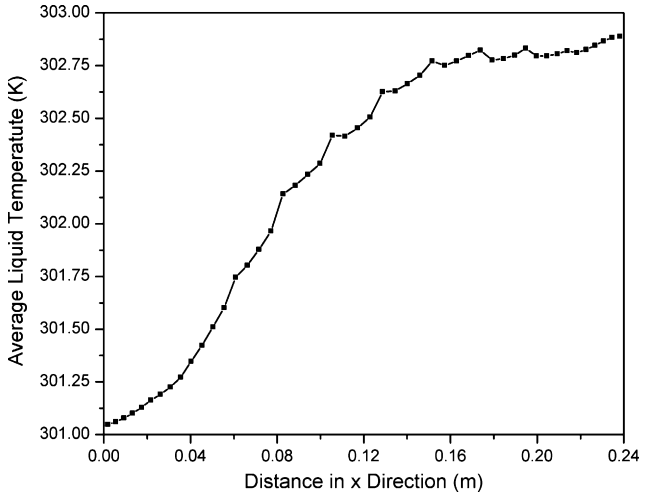

Fig. 11. Average liquid temperature in a y–z plane as a function of the x direction for liquid weir load, Q_l/W, equal to 1.2×10^{-3} m^3/s m at 298.15 K and the superficial gas velocity, U_g, equal to 0.7 m/s at 318.18 K.

the distillation sieve tray performance in terms of heat and mass transfers.

5. Concluding remarks

The main results show temperature and volume fraction profiles as a function of time and position in the sieve tray and confirm that the major difficulty in sieve tray gas–liquid flow modelling is due to several flow regimes. Therefore, efficient constitutive equations for calculating interphase momentum, heat and mass transfers are necessary, in order to minimize the errors derived from the use of empirical correlations. The main conclusion of this work is that the gas–liquid flow in distillation sieve trays presents a chaotic characteristic for the properties, which are intensified by the increment of the superficial gas velocity. Equal velocity in all hole entrances can be assumed as a simplification model, since the gas inlet boundary condition analysis showed no sensitivity to this simplification. It was also possible to identify hot and cold regions near to the liquid entrance and weir, respectively. So, the methodology proposed showed to be adequate, with capability to describe, from CFD techniques, the thermal gas–liquid flow on a sieve tray distillation. The next step will be to insert the mass transfer equations in the model. Finally, the CFD tools presented and discussed in this work make it possible to know better the turbulent thermal gas–liquid flow on a sieve tray of distillation columns and they can be used to optimize design and operating conditions of such processes.

Acknowledgements

The authors acknowledge CNPq and Fapesp for the financial support.

References

[1] E.J. Henley, J.D. Seader, Equilibrium-Stage Separation Operations in Chemical Engineering Ed., Wiley, New York, 1981.
[2] F.J. Zuiderweg, Sieve trays: a view on the state of the art, Chem. Eng. Sci. 37 (1982) 1441–1464.
[3] H.Z. Kister, Distillation Design, McGraw-Hill, New York, 1992.
[4] R. Krishnamurthy, R. Taylor, A nonequilibrium stage model of multicomponent separation processes—Part I: model description e method of solution, AIChE J. 31 (1985) 456–465.
[5] A.A.C. Barros, M.H. Pescarini, M.R. Wolf Maciel, Development of a software for simulation separation processes using a nonequilibrium stage model, Comp. Aided Process Eng. (1996) 279–284.
[6] C.J. Colwell, Clear liquid height and froth density on sieve tray, Ind. Eng. Chem. Proc. Des. Dev. 20 (1979) 298.
[7] D.L. Bennett, R. Agrawal, P.J. Cook, New pressure drop correlation for sieve tray distillation columns, AIChE J. 26 (1983) 434–442.
[8] G.E. English, M. van Winkle, Efficiency in bubble cap distillation columns, Chem. Eng. Sci. 70 (1983) 241–246.
[9] R.L. Bell, R.B. Solari, Effect of nonuniform velocity fields and retrograde flow on distillation tray efficiency, AIChE J. 19 (1983) 688.
[10] R.B. Solari, R.L. Bell, Fluid flow patterns and velocity distribution on commercial-scale sieve tray, AIChE J. 32 (1986) 640–648.
[11] M.L. Bertodado, Two fluids for two-phase turbulent jets, Nucl. Eng. Des. 179 (1998) 65–74.
[12] H.F. Meier, J.J.N. Alves, M. Mori, Comparison between staggered and collocated grids in the finite-volume method performance for single and multi-phase flows, Comp. Chem. Eng. 23 (1999) 247–262.
[13] H.F. Meier, K. Ropelato, K.H. Forster, J.J. Iess, M. Mori, Computational Fluid Dynamics (CFD) for Cyclone Evaluation and Design, Part 1, ZKG International 55 (2002) 64–75.
[14] J.J.N. Alves, M. Mori, Fluid dynamics modelling and simulation of circulating fluidized bed reactors: analyses of particle phase stress models, Comp. Chem. Eng. 22 (1998) 763–766.
[15] C.K.K. Lun, Numerical simulation of dilute turbulent gas-solid flows, Int. J. Multiphase Flow 26 (2000) 1707–1736.
[16] Y. Cheng, F. Wei, Y. Guo, Y. Jin, W. Lin, Inlet and outlet effects on flow patterns in gas-solid risers, Powder Technol. 98 (1998) 151–156.
[17] A. Cockx, Z. Do-Quang, A. Liné, M. Roustan, Use of computational fluid dynamics for simulating hydrodynamics and mass transfer in industrial ozonation towers, Chem. Eng. Sci. 54 (1999) 5085–5090.
[18] Y. Cheng, F. Wei, Y. Guo, Y. Jin, CFD simulation of hydrodynamics in the entrance region of a downer, Chem. Eng. Sci. 56 (2001) 1687–2001.
[19] N. Boisson, M.R. Malin, Numerical prediction of two-phase flow in bublle columns, Int. J. Numer. Methods Fluids 23 (1996) 1289–1310.
[20] R. Krishna, J.M. van Baten, Mass transfer in bubble columns, Catal. Today 79–80 (2003) 67–75.
[21] R. Krishna, J.M. van Baten, M.I. Urseanu, Three-phase eulerian simulations of bubble column reactors operating in the churn-turbulent regime: a scale up strategy, Chem. Eng. Sci. 55 (2000) 3275–3286.
[22] R. Krishna, J.M. van Baten, M.I. Urseanu, J. Ellenberger, Design and scale up of a bubble column slurry reactor for Fischer-Tropsch synthesis, Chem. Eng. Sci. 56 (2001) 537–545.
[23] E. Delnoij, J.A. Swaaij, W.P.M. Kuipers, Dynamic simulation of gas-liquid two-phase flow: effect of column aspect ratio on flow structure, Chem. Eng. Sci. 52 (1997) 3759–3772.
[24] E. Delnoij, J.A. Kuipers, W.P.M. Swaaij, A three-dimensional CFD model for gas-liquid bubble columns, Chem. Eng. Sci. 54 (1999) 2217–2226.
[25] V. Michele, D.C. Hempel, Liquid flow and phase holdup-measurement and CFD modeling for two-and three-phase bubble columns, Chem. Eng. Sci. 57 (2002) 1899–1908.
[26] Y. Pan, M.P. Dudukovic, M. Chang, Dynamic simulation of bubble flow in bubble columns, Chem. Eng. Sci. 54 (1999) 2481–2489.
[27] D. Pfleger, S. Becker, Modelling and simulation of the dynamic flow behaviour in a bubble column, Chem. Eng. Sci. 56 (2001) 1737–1747.
[28] A. Sokolichin, G. Eigenberger, Applicability of standart k-ε turbulence model to the dynamic simulatin of buble columns: Part I. Detailed numerical simulations, Chem. Eng. Sci. 54 (1999) 2273–2284.
[29] P. Spicka, M.M. Dias, J.C.M. Lopes, Gas-liquid flow in a 2D column: comparison between experimental data and CFD modelling, Chem. Eng. Sci. 56 (2001) 6367–6383.

[30] D. Wiemann, F. Lehr, D. Mewes, Numerical calculation of the flow field in a bubble column considering the absorption of the gas phase, in: International Conference on Distillation and Absorption, Baden-Baden, 2002 (CD-Rom).
[31] B. Mehta, K.T. Chuang, K. NandaKumar, Model for liquid phase flow on sieve tray, Trans. I, Chem. Eng. 76 (1998) 843–848.
[32] C.J. Liu, X.G. Yuan, K.T. Yu, X.J. Zhu, A fluid-dynamic model for flow pattern on a distillation tray, Chem. Eng. Sci. 55 (2000) 2287–2294.
[33] R. Krishna, J.M. van Baten, J. Ellenberger, A.P. Higler, R. Taylor, CFD simulation of sieve tray hydrodynamics, Chem. Eng. Res. Des., Trans IChenE 77 (1999) 639–646.
[34] J.M. van Baten, R. Krishna, Modelling sieve tray hydraulics using computational fluid dynamics, Chem. Eng. J. 77 (2000) 143–151.
[35] C. Soares, D. Noriler, A.A.C. Barros, H.F. Meier, M.R. Woilf Maciel, Computational fluid dynamics for simulation of gas-liquid flow on a sieve plate: model comparisons, in: International Conference on Distillation and Absorption, Baden-Baden, 2002 (CD-Rom).
[36] D. Noriler, M.Sc. thesis, Laboratory of Separation Process Development, State University of Campinas, Campinas, São Paulo, Brazil (2003).
[37] G. Gesit, K. Nandakumar, K.T. Chuang, CFD modeling of flow and hydraulics of commercial-scale sieve trays, AIChE J. 49 (4) (2003) 910–924.
[38] R.B. Bird, W.E. Stewart, E.N. Lightfoot, Transport Fenomena. Ed., Wiley, New York, 1960.
[39] W.E. Ranz, W.R. Marshall, Chem. Eng. Progr. 48 (3) (1952) 141.